Year 2010

Resume

of the thesis

PRESSURE-INDUCED COLLISIONAL PARAMETERS OF ROVIBRATIONAL LINES OF WATER VAPOUR AND OZONE

presented to
the U.F.R. Sciences et Techniques of the University of Franche-Comte

to obtain a PhD degree in Physics

by
MISHINA Tatiana Petrovna

Defended on 17 December 2010

Examination Commission:

President	M L.N. Sinitsa	Professor, Laboratory of Molecular Spectroscopy, Institute of Atmospheric Optics, Tomsk
Reviewers	Mme A. Perrin	Director of Researches, Interuniversitairy Laboratory of Atmospheric Systems, University Paris-12
	M V.I. Perevalov	Professor, Laboratory of Theoretical Spectroscopy, Institute of Atmospheric Optics, Tomsk
Examinators	M V. Ballenegger	Associate Professor, University of Franche-Comte
	Mme J.V. Buldyreva	Associate Professor, University of Franche-Comte
	M A.D. Bykov	Professor, Laboratory of Molecular Spectroscopy, Institute of Atmospheric Optics
	Mme N.N. Lavrentieva	Director of Researches, Laboratory of Molecular Spectroscopy, Institute of Atmospheric Optics

Table of contents

Introduction

Current importance of the work

The information about rotation-vibration spectral lines is used in different fields of science such as atmospheric studies, laser and flame physics, *etc*. Spectral line shape parameters due to the pressure of atmospheric gases allow studies of collisions dynamics and determination of the intermolecular interaction potential. Consequently, a lot of line parameter measurements covering a wide spectral region from the microwave to visible domains have been made [1-10].

The first practically convenient method for semi-classical calculation of half-widths and shifts of isolated spectral lines was developed by Anderson [11] and reformulated by Tsao and Curnutte [12]. It is referred to in the literature as the Anderson–Tsao–Curnutte (ATC) theory.

The principal drawback of the ATC theory – the artificial cut-off procedure to avoid the divergence of the interruption function for small intermolecular distances – initiated development of improved semi-classical methods. The most known and popular of them is the Robert–Bonamy (RB) formalism [13] based on the linked cluster theorem [14] and using parabolic trajectories curved by the isotropic potential. Later a model of exact classical trajectories [15] has been introduced in the RB approach (RBE method) [16-18].

This theorem enables an exponential representation of the collision matrix elements and yields finite values of the interruption function for small values of the impact parameter. However, the terms are usually retained to the second-order only. Attempts to improve the calculations require adding more terms which also diverge at short distances so that the results of term-by-term summation are really indefinite. Thus, at a deeper insight, the problem of the summation of the perturbing theory series steel remains in the RB formalism.

Recently, Ma, Tipping and Boulet [19] revisited the derivation of the RB expressions and discovered that the use of the linked cluster theorem is not valid for the diagonal matrix element $\langle\langle f2i2|S|f2i2\rangle\rangle$. The general structure of the RB equations can be however kept if the average on the bath molecules is taken as the cumulant average. For strongly interacting molecular systems the modified expressions lead to an observable change in the line width values and to a drastic change of the line shifts; the agreement with experimental data was however surprisingly worse.

The same authors (with some new collaborators) tried to estimate the importance of the vibrational dependence of classical trajectories [20] which is typically ignored in the RB formalism (active molecule in the initial and final vibrational states is supposed to follow the same classical path). Their study realized for H_2-He system with a strong vibrational dephasing

revealed the non-negligible character of this vibrational dependence for the 1st-order line shifts. No improvement was obtained for the line widths defined principally by the second-order contributions (vibrational dependence of the trajectories for these terms was completely neglected by the authors).

Quite expensive CPU cost of semi-classical RB calculations for active molecules with many vibrational modes and many branches in their IR spectra initiated the development of a semi-empirical method similar to the ATC-theory but including correction factors [21]. These factors allow accounting for the trajectory curvature, vibrational effects and correction to the scattering matrix. The necessary fitting parameters are determined from some available experimental data.

Like the ATC theory, this method is characterised by a clear physical meaning and a possibility to calculate separately the contributions of different types of intermolecular interactions and different scattering channels to the collisional line shape parameters. The last aspect allows an analysis of the vibration-rotational dependence of line broadening and shifting coefficients. Since the linewidths are practically not sensitive to the vibrational dependence, the semi-empirical approach gives the possibility to make numerous calculations of the line shape parameters without a noticeable loss of precision.

However, there is no universal method to calculate the collisional parameters of rovibrational spectral lines in different spectral regions, so that theoretical methods require constantly further improvements.

For active molecules with small values of rotational constants rovibrational lines are not very well isolated and start to overlap even at moderate pressures. This overlapping called also “line mixing” or “line interference” has an influence on the absorption, emission and Raman scattering spectra and leads to an increased absorption in the atmospheric microwindows. The interference influence on the line shift is small for most water vapour lines. However, this influence can be significant for the lines whose upper vibrational–rotational states are in a strong resonance. It is therefore necessary to evaluate the contribution of the line interference in the absorption of radiation for different atmospheric paths (vertical and slant) as well as for summer and winter conditions.

Purposes of the work

The goals of the present work are focused on improvements or testing the existing semi-classical methods for collisional line width and shift calculations. The main tasks of this work are:

1. Modification of the calculation method for the resonance functions by the use of the generalised Euler transformation in order to obtain broadening and shifting coefficients of spectral lines.
2. Semi-classical and semi-empirical calculations of ozone line widths broadened by nitrogen and oxygen and a study of the vibrational dependence of classical trajectories for the pure vibrational contribution to the ozone line shifts, aiming to improve their values included in spectroscopic data banks.
3. Determination of semi-empirical parameters and calculation of broadening and shifting coefficients of water vapour lines for spectroscopic databases.
4. Study of the interference of water vapour spectral lines and evaluation of its influence on the atmospheric transmission for vertical and slanted paths.

New results obtained:

1. Using the generalized Euler transformation for the summation of divergent series allowed obtaining a convergent expression of the interruption (or "efficiency") function and calculation of new resonance functions in the cases of strong (HF-HF) and weak (CO-CO) dipole-dipole and dipole-quadrupole (HF-N_2) interactions.
2. Nitrogen- and oxygen-broadening coefficients of ozone lines were calculated by semi-classical RBE and semi-empirical methods for the $\nu_1+\nu_3$ band.
3. Vibrational dependence of classical trajectories was studied for the 1^{st}-order contribution to the rovibrational shifts of O_3-N_2 lines in the framework of semi-classical RB approach with exact trajectories and vibrational dependence of isotropic potential coming from the O_3 dipole moment and polarizability.
4. Values of effective dipole polarizability in excited vibrational state were obtained for all vibrational bands of water vapour experimentally studied in the literature.
5. Collisional parameters of water vapour spectral lines were calculated for highly excited ro-vibrational states up to the dissociation limit of 25000cm^{-1}.
6. Interference of water vapour spectral lines is shown to lead to noticeable error in computation of atmospheric absorption coefficient for slanting atmospheric paths for winter conditions of mid-latitude atmosphere model and to the disappearance of microwindow region for increasing zenithal angle.

Scientific importance of the work

As a rule, the interruption function represents a perturbation series, which is divergent for small values of the impact parameter. Therefore, the use of the generalised Euler transformation allows avoiding the cut-off procedure and obtaining a correct asymptotic behaviour of the interruption function and calculation of new resonance functions. New resonance functions obtained by the generalized Euler transformation can be used for obtaining broadening and shifting coefficients in the case of strong molecular collisions when the straight-path approximation is applied. These functions take into consideration all collision factors and can be used for all linear molecules.

Use of exact trajectory model in the RB formalism leads to a better agreement with experimental data for ozone spectral lines broadened by N_2 and O_2 pressure. The semi-empirical method gave also very good results for reproducing the line widths in the $\nu_1+\nu_3$ band and opened a perspective of their easy calculation for all other vibrational bands.

Taking into account the vibrational dependence of the classical trajectories allows evaluation of its importance for shifting coefficients of the O_3-N_2 spectral lines.

The semi-empirical method gives the values of broadening and shifting coefficient of rovibrational spectral lines of water molecule which agree favourably with experimental and other theoretical data and enables therefore a reliable prediction of collisional line shape parameters.

Since the interference influence of water vapour spectral lines gives a significant contribution to weakening of atmosphere radiation, it is necessary to take into account this interference.

Practical use of the work:

The calculated line broadening and shifting coefficients as well as their temperature exponents are included in the "ATMOS" Information System and spectroscopic data basis GEISA.

The results obtained in this work are published in scientific journals and presented at the national and international conferences:

- International Symposium "Atmospheric and Ocean Optics. Atmospheric Physics": Tomsk (2004, 2006, 2009, 2010), Ulan-Ude (2007), Krasnoyarsk (2008);
- International Symposiums on High Resolution Molecular Spectroscopy HighRus-2006 and HighRus-2009,
- IV Russian conference "Material engineering, technologies and ecology in the 3^{d} millennium (Tomsk, 2009),

— XI^{èmes} Journées des Écoles Doctorales Louis Paster – Université de Franche-Comté et Carnot – Université de Bourgogne (Besançon, 2010),
— VII Russian Symposium «Control of environment and climate 2010» (Tomsk, 2010).

Acknowledgments

This work is supported by the Russian Foundation for Basic Research (grant 08-02-12061-ofi, grant 05-07-90196, Russian Research grants 112-001-020 and 09-05-00889-a), Russian Academy of Sciences, program “Optical Spectroscopy and Frequency Standarts”, NERC, grant of the Royal Society of Great Britain 2006/R3 IJP, INTAS grant 03-51-3394, French program “Les Enveloppes Fluides et l’Environnement – CHimie Atmospherique (LEFE-CHAT)”, as well as European Community (grant FP6 MCA IIF WWLC-980021).

Chapter I

Impact theory of broadening and shifting of spectral lines by pressure of atmospheric gases

I.1. Semi-classical theory of Anderson–Tsao-Curnutte and semi-empirical method

It is well known that the impact approximation assumes binary collisions between the radiating and perturbing molecules, and a short duration of collisions in comparison with the time between collisions. In his pioneering paper [11] Anderson also supposed that the classical molecular trajectories could be approximated by straight-line paths. The time-evolution operator that describes the collision dynamics was expanded in a perturbation series by means of standard time-dependent perturbation theory. This theory was further reformulated in a simpler manner by Tsao and Curnutte [12], so that in the current literature the approach is usually referred to as Anderson–Tsao–Curnutte (ATC) theory.

In the ATC theory the half width γ_{fi} and shift δ_{fi} of the spectral line corresponding to the optical transition $i \rightarrow f$ are given by

$$\gamma_{fi} + i\,\delta_{fi} = \frac{n}{c}\sum_{r}\rho\,(r)\int_{0}^{\infty} d\,v\; v\;\; f\,(v)\int_{0}^{\infty} db\, b\, S\,(b)\,, \tag{1.1}$$

where n is the density of perturbing molecules; r is the ensemble of quantum numbers of the perturbing molecule; $\rho(r)$ is the occupation number of the perturbing molecule; v is the relative collision velocity; $f(v)$ is the Maxwell velocity distribution function and $S(b)$ is the efficiency function for collisions with the impact parameter b:

$$S(b) = S_1(b) + S_2(b) + \ldots. \tag{1.2}$$

Usually only the first- and second-order terms of this expansion are retained. The first-order term in Eq. (1.2) is purely imaginary and gives contribution to the line shift only. It depends on the difference between the mean values of isotropic potential in the upper and lower vibrational states. In the second-order, there are two types of contributions, the well known “outer” and “middle” terms, which give rise both to the width and shift. The second-order contribution

depends on the strengths of transitions induced by collisions and degree of fulfilment of resonance condition.

$$S_2(b) = S_{2,i}(b)_{outer} + S_{2,f}(b)_{outer} + S_2(b)_{middle}. \tag{1.3}$$

When b is small the collision is very strong and the second-order term diverges. It means that the radiation is completely interrupted by the transition of the molecule to a different nondegenerate state or that an arbitrary phase-shift occurs even if the molecule remains in the same nondegenerate state. In each case, it is assumed that for these small values of b ($b \leq b_0$)

$$S_2(b) = 1, \tag{1.4}$$

and the interruption (cut-off) parameter b_0 the in determined from the condition

$$\mathrm{Re}\, S(b_0) = 1 \tag{1.5}$$

(in the initial Anderson's work only the line widths were considered).

Many calculations were performed on the basis of expansion (1.2) resulting in satisfactory agreement with experimental data for the case of polar colliding molecules having large dipole moments. For polar molecules colliding with atoms or non-polar molecules the ATC-calculated line widths were however not satisfactory.

Many alternative approaches were suggested in order to avoid the using of Anderson's interruption procedure. The most recent of them is the semi-empirical method proposed several years ago [21]. This method is based on the ATC theory which is improved by introducing correction factors with model parameters determined by fitting the calculated broadening and/or shifting coefficients to some experimental data. These factors account for the trajectory curvature, vibrational effects and corrections to the scattering matrix. The semi-empirical method allows also separate calculation of contributions from different types of intermolecular interactions and different scattering channels, an analysis of vibration-rotational dependence of line broadening and shifting coefficients as well as easy numerous calculations of line shape parameters without a noticeable loss of precision.

The half-width of a spectral line in the ATC theory can be written as

$$\gamma_{fi} = A(f,i) + \sum_l \sum_{i'} D^2(ii'|l) P_l^{ATC}(\omega_{ii'}) + \sum_l \sum_{f'} D^2(ff'|l) P_l^{ATC}(\omega_{ff'}), \tag{1.6}$$

where $A(f,i)=\frac{n}{c}\sum_r \rho(r)\int_0^\infty v dv b_0^2(v,r,i,f)$ is the term coming from the cut-off procedure, $D^2(ii'|l)$ are transition strengths and the expansion coefficients $P_\ell^{ATC}(\omega_{ii'})$ are so-called interruption or efficiency functions. These functions depend on the properties of perturbing and radiating molecules and are determined by the intermolecular potential, relative trajectories as well as the energy levels and wave functions of the perturbing molecule. Since $D^2(ii'|l)$ are well known, the correction factor $C_\ell(\omega)$ introduced by the semi-empirical method is applied to the interruption functions:

$$P_l(\omega)=C_l(\omega)P_l^{ATC}(\omega), \tag{1.7}$$

and the usual choice of $C_\ell(\omega)$:

$$C_l(\omega)=\frac{c_1}{c_2\sqrt{J}+1}, \tag{1.8}$$

is completely defined by the fitting parameters c_1, c_2. The parameter c_1 includes a correction connected with the using of ATC-theory interruption procedure and the parameter c_2 allows taking into account vibrational dependence of line shape parameters.

Once determined from fitting to experimental data, these parameters c_1 and c_2 enable reproducing of line widths in all other vibrational bands, since the vibrational dependence of line broadening coefficients is known to be weak.

I.2. Semi-classical formalism of Robert–Bonamy and its modifications by Ma–Tipping–Boulet

The principal drawbacks of the ATC theory (straight-line trajectories appropriate solely for long-range interactions, perturbation series for the scattering matrix resulting in the obligatory but unphysical cut-off procedure) are easily overcome in the framework of the semi-classical formalism developed by Robert and Bonamy [13].

The using of the linked cluster theorem in this approach allows an exponential representation of the collision matrix elements with an infinite series of Eq. (1.2) as argument. This representation leads to finite values of $S(b)$ for small values of the impact parameter if a restricted number of terms is taken into account. The evaluation of the exact sum (necessary for improving calculations) requires more terms of the series. It is obvious, that the complete series diverges at short distances likely the ATC series (1.2), so that the results of term-by-term summation are indefinite and the problem of summation of the perturbation theory series steel remains.

In the formalism of Robert and Bonamy [13] the line half-width γ_{fi} and the line shift δ_{fi} are determined as

$$\gamma^{RB}{}_{fi} = \frac{n}{c}\sum_r \rho(r)\times$$

$$\times\int_0^\infty dv\, v\, f(v)\int_0^\infty db\, b\left\{1-\left[1-S^{(L)}_{2,f2i2}\right]e^{-\left(S_{2,f2}+S_{2,i2}+S^{(C)}{}_{2,f2i2}\right)}\cos\left[\left(S_{1,f2}+S'_{2,f2}\right)-\left(S_{1,i2}+S'_{2,i2}\right)\right]\right\},$$

(1.9)

$$\delta^{RB}{}_{fi} = \frac{n}{c}\sum_r \rho(r)\times$$

$$\times\int_0^\infty dv\, v\, f(v)\int_0^\infty db\, b\left\{\left[1-S^{(L)}_{2,f2i2}\right]e^{-\left(S_{2,f2}+S_{2,i2}+S^{(C)}{}_{2,f2i2}\right)}\sin\left[\left(S_{1,f2}+S'_{2,f2}\right)-\left(S_{1,i2}+S'_{2,i2}\right)\right]\right\}.$$

(1.10)

The superscripts (L) and (C) on the second-order contributions S_2 correspond to the "linked" and "connected" elements of the linked cluster theorem. The first order contributions S_1 are defined by the isotropic part of the potential, whereas the second order contribution S_2 are described by its anisotropic part.

Instead of approximate parabolic trajectories of the traditional RB formalism, Bykov et al [22] proposed to use exact solutions of classical equations of motion for a particle in an isotropic potential field [15]. However no calculation of line widths had been performed by the authors. This model of exact trajectories has been incorporated in the RB-calculation of line widths for linear molecules, symmetric and asymmetric tops by Buldyreva et al [16-18].

Ma, Tipping and Boulet [19] have found an invalid assumption in the RB formalism connected with the using of the cumulant expansion for the diagonal matrix element $\left\langle\left\langle f2i2|S|f2i2\right\rangle\right\rangle$. Authors have suggested considering an average over the internal degrees of a

perturbing molecule as the cumulant average (Modified RB formalism – MRB). Therefore the final formulae for calculations of line shape parameters look like the formula of the RB formalism:

$$\gamma^{MRB} = \frac{n}{c}\int_0^\infty v\, f(v)\, dv \int_0^\infty db\, b \left\langle 1 - \cos\left(\left\langle S_1 \right\rangle_r + \mathrm{Im}\left\langle S_2 \right\rangle_r \right) \mathrm{e}^{-\mathrm{Re}\langle S_2 \rangle_r} \right\rangle \qquad (1.11)$$

$$\delta^{MRB} = \frac{n}{c}\int_0^\infty v\, f(v)\, dv \int_0^\infty db\, b \left\langle \sin\left(\left\langle S_1 \right\rangle_r + \mathrm{Im}\left\langle S_2 \right\rangle_r \right) \mathrm{e}^{-\mathrm{Re}\langle S_2 \rangle_r} \right\rangle \qquad (1.12)$$

To evaluate the differences introduced by their modifications, the authors calculated line widths and line shifts for HF-N_2 and HF-HF molecular systems, characterized respectively by weak and strong interactions. For the weakly interacting HF-N_2 system, no important differences with the standard RB calculations were observed. For the strongly interacting HF-HF system the line widths were obviously changed, and for the line shifts this change was drastic. However, the agreement of MRB results with experiment was worse.

Ma, Tipping and Boulet [20] studied also the importance of the vibrational dependence of classical trajectories, which are tacitly supposed to be vibrationally-independent in the RB formalism. Their study was focused on the H_2-He system, for which vibrational dephasing give the main contribution to the first-order vibrational shift. They tested straight-line, parabolic and exact trajectories and obtained a better agreement with their new quantum-mechanical calculations for the line shift at various temperatures (the agreement with experiment was worse). Since they completely neglected (!) the vibrational dependence of trajectories when calculating the second-order terms, for the line widths (due mainly to S_2) their results were even farther from experimental data then for the usual vibrationally independent trajectories.

I.3. Intermolecular interaction potential

The intermolecular potential includes all possible types of interactions between molecules.

The long-range electrostatic contribution is due to the charges distributions of colliding molecules and is generally expressed through the dipole, quadrupole and higher moments (subscripts 1 and 2 refer to the radiating and perturbing molecules, respectively):

$$V^{el} = \sum_{l_1 l_2 l\, n_1 n_2} \sum_{m_1 m_2 m_3} \sum_{w,q} \frac{U(l_1 l_2 l\, n_1 n_2 w q)}{R^{q+l_1+l_2-2w}} \otimes C(l_1 l_2 l; m_1 m_2 m) D^{l_1}_{m_1 n_1}(\Omega_1) D^{l_2}_{m_2 n_2}(\Omega_2) Y_{l\,m}(\omega), \quad (1.13)$$

where l_1, l_2, l are the tensorial ranks of the molecular moments and of their tensorial product ($l=l_1+l_2$ here) which determine the symmetry of the interaction; n_1, n_2 are the projections of the angular momenta $\vec{J}_1, \vec{J}_2$ along the laboratory z-axis; m_1, m_2 are the projections of $\vec{J}_1, \vec{J}_2$ along the molecular z-axes; $C(l_1 l_2 l; m_1 m_2 m)$ is the Clebsch-Gordan coefficient; $D^{l_1}_{m_1 n_1}(\Omega_1)$, $D^{l_2}_{m_2 n_2}(\Omega_2)$ are the rotation matrices, where $\Omega_1 = (\alpha_1, \beta_1, \gamma_1)$ and $\Omega_2 = (\alpha_2, \beta_2, \gamma_2)$ are the Euler angles describing the orientation of the molecular axes relative to the laboratory axes; $Y_{lm}(\omega)$ is the spherical harmonics describing the orientation of the intermolecular distance vector $\vec{R}$ in the laboratory frame. The radial components *U(...)* and the powers w and q (integers) depend on the considered interactions.

The next types of long-range molecular interactions usually taken into account are the induction and dispersion terms determined by dipole moment and dipole polarizability.

Although an electrostatic potential is suitable for large intermolecular separations, it is clearly inadequate at short range for neutral molecules. The electrostatic terms in Eq. (1.13) are always orientation-dependent, whereas molecules in any orientation must ultimately repel one another at close range. In order to include short-range forces, the electrostatic contributions are completed by so-called atom-atom pairwise interactions in the Lennard-Jones form:

$$V^{at-at} = \sum_{i=1}^{n} \sum_{j=1}^{m} 4\varepsilon_{ij} \left\{ \frac{\sigma_{ij}^{12}}{r_{1i,2j}^{12}} - \frac{\sigma_{ij}^{6}}{r_{1i,2j}^{6}} \right\}, \quad (1.14)$$

where subscripts 1i and 2j refer to the ith atom of molecule 1 and the jth atom of molecule 2, n and m are the number of atoms in molecules 1 and 2, respectively, and ε_{ij} and σ_{ij} are the Lennard-Jones parameters for the atomic pairs. The positive terms ($\sim r_{1i,2j}^{-12}$) in Eq. (1.13) represent the repulsive forces at close intermolecular distances, whereas the negative terms on $r_{1i,2j}^{-6}$ describe (approximately) the contributions coming from long-range induction and dispersion interactions.

The full interaction potential (short- and long-range interactions) contains isotropic and anisotropic parts

$$V = V_{iso} + V_{aniso} \quad (1.15)$$

The isotropic part is due to the short-range forces and long-range induction and dispersion terms; (within the atom-atom potential model, V_{iso} is obtained taking the contribution with $l_1=l_2=l=0$ in Eq. (1.13)). For the long-range part only, the isotropic components are determined by the dipole moment of the active molecule and the dipole polarizabilities:

$$V_{iso}^{ind} = -\frac{\mu_1^2 \alpha_2}{r^6} \qquad V_{iso}^{dis} = -\frac{3}{2}\frac{I_1 I_2}{I_1 + I_2}\frac{\alpha_1 \alpha_2}{r^6}, \qquad (1.16)$$

where μ_1 is the dipole moment of radiating molecule and α and I are the polarizability and ionization potential for radiating and perturbing molecules. When the vibrational dependence of V_{iso} is of interest, it is included via μ_1 and α_1. This isotropic part of the potential is typically used to govern the classical trajectories for the relative molecular motion.

Chapter II

Use of the generalized Euler series transformation for calculation of widths and shifts of molecular spectral lines

The impact approximation, the perturbation theory and a representation of interruption function as a power series of interaction are widely used in calculations of collisional line widths and shifts. For small values of the impact parameter the intermolecular interaction becomes strong and the perturbation series is expected to diverge [12]. This problem represented the main goal of many studies (see, for instance, [23-26] and references therein) and several approaches were developed to overcome the perturbation series divergence. The use of the generalized Euler transformation allows also solving this problem. The full resonance approximation is employed as a starting point and a convergent expression similar to the ATC formulae is obtained for the interruption function at short intermolecular distances [1*] (Appendix A). This approach gives true sum values for the convergent series, if the chosen approximation function is close enough to the approximated function.

II.1. The generalized Euler series transformation

In order to compute the series sum by the Euler method it is necessary to use an approximate expression for the interruption function, which conserves its main asymptotic characteristics.

Let the series expansion of the function $f(z)$

$$f(z) = \sum_{n=0}^{\infty} f_n z^n \tag{2.1}$$

can be approximated by a known function $g(z)$:

$$f(z) \approx g(z) = \sum_{n=0} g_n z^n = g_0 + g_1 z + g_2 z^2 + \ldots . \tag{2.2}$$

The Euler method allows expressing of Eq. (2.1) in the form:

$$f(z) = \sum_{n=0}^{\infty} (-1)^n D_n \Phi_n(z), \tag{2.3}$$

where

$$\Phi_n(z) = \frac{z^n}{n!}\frac{d^n g(z)}{d\,z^n}, \tag{2.4}$$

and

$$D_n = \sum_{r=0}^{n}(-1)^r \binom{n}{r} a_r, \qquad a_r = f_r / g_r \tag{2.5}$$

When r tends to infinity, the ratio f_r/g_r tends to one, and the transformed series converges [21→26].

II.2. Calculation of resonance functions

In order to compute the series sum (1.2) by the Euler method it is necessary to use an approximate expression for the interruption function with the asymptotic characteristics $S(b)\,|_{b\to 0} \to 1$ and $S(b)\,|_{b\to\infty} \to 0$. A parameter λ is introduced in the series of Eq. (1.2); after summation this parameter will be put to 1. The interruption function and the approximate expression for its real part are given, respectively, by

$$S(b,\lambda) = S_0 + \lambda\, S_1 + \lambda^2 S_2 + \lambda^3 S_3 + \lambda^4 S_4 + \ldots, \tag{2.6}$$

and

$$\mathrm{Re}\,S(b) = G(\lambda)\,|_{\lambda\to 1} = 1 - \cos\left(\lambda\,\frac{S_1}{b^5}\right)\cdot\exp\left(-\lambda^2\,\frac{\mathrm{Re}\,S_2}{b^4}\right)|_{\lambda\to 1}. \tag{2.7}$$

To obtain the expression for the transformed series the generalized Euler series transformation

$$\sum_{n=0}^{\infty} D_n\,\frac{\lambda^n}{n!}\frac{d^n G(\lambda)}{d\lambda^n} = \sum_{r=0}^{\infty} S_r(b)\,P_r(b), \tag{2.8}$$

is used, where

$$P_r(b) = \sum_{n=r}^{\infty}(-1)^{n+r}\binom{n}{r}\frac{\lambda^n}{n!}\frac{d^n G(\lambda)}{d\lambda^n}\frac{1}{g_r} \tag{2.9}$$

are corrections for the ATC functions and

$$\binom{n}{r} = n!/\,r!(n-r)! \tag{2.10}$$

is the binomial coefficient.

In the integral on the impact parameter $S(b)$ contains the resonance functions f_{nm} (n, m – are the indexes of electrostatic moments, i.e. n or m equal 1 for dipole radiation, n or m equal 2 for quadrupole radiation, etc.) and the correction factor $P(b)$ is a multiplier for them. The "new" resonance functions $\tilde{f}_{nm}$ read

$$\tilde{f}_{nm}(k) = f_{nm}\left(\frac{2\pi\, cb}{v}\omega\right)P_r(b), \tag{2.11}$$

where k is the so-called resonance parameter (Messy parameter).

The zero-order approximation of the interruption function, the correction for the dipole-dipole resonance function and "new" resonance functions for the self-broadened lines of the strongly interacting HF-HF system are presented, respectively in Figs 1-3. Figures 4-5 show the resonance functions for CO-CO system with weak dipole-dipole interaction and HF-N_2 system with leading dipole-quadrupole interaction.

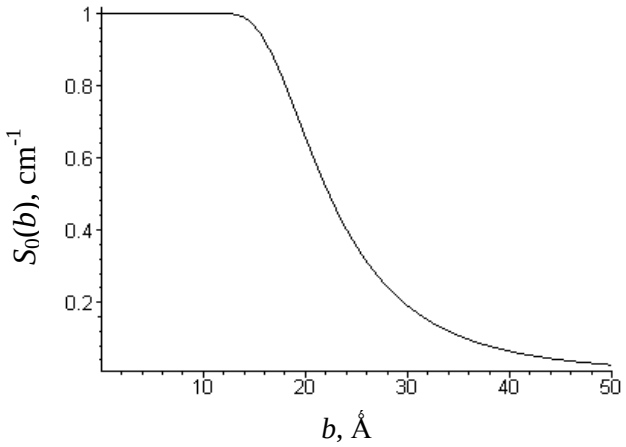

Fig. 1. The zero-order approximation of the interruption function in function of the impact parameter for the self-broadened HF lines.

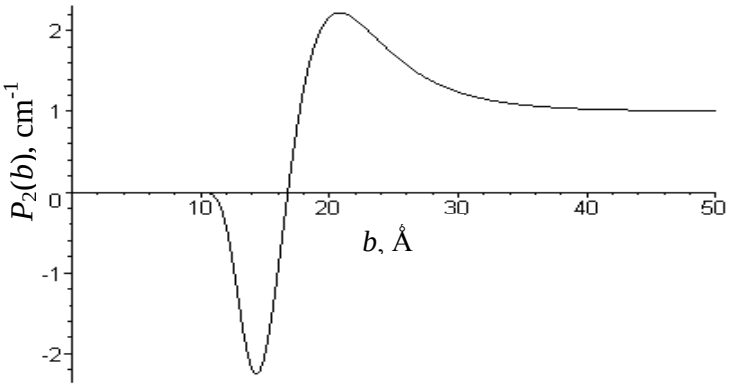

Fig. 2. The second-order correction for the dipole-dipole HF-HF resonance function in function of the impact parameter.

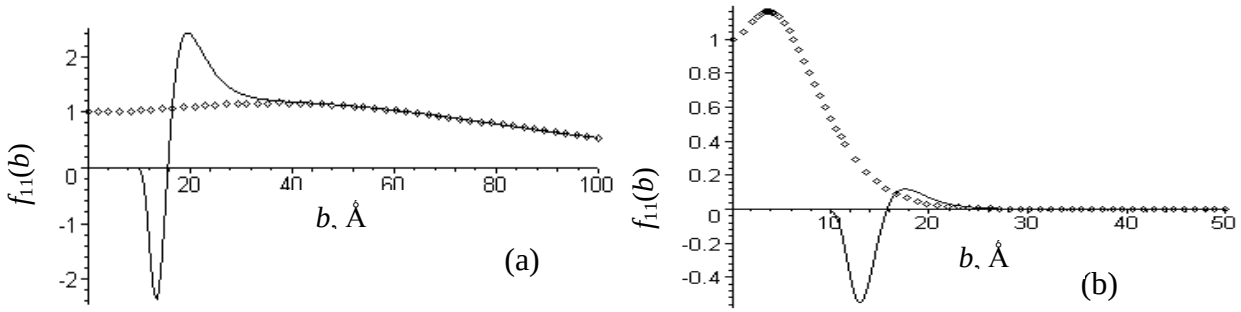

Fig. 3. The resonance function for the dipole-dipole interaction of the HF-HF system for the transition frequencies of 1cm^{-1} (a) and 10 cm^{-1} (b): °° - "old" resonance function, __ - "new" resonance function.

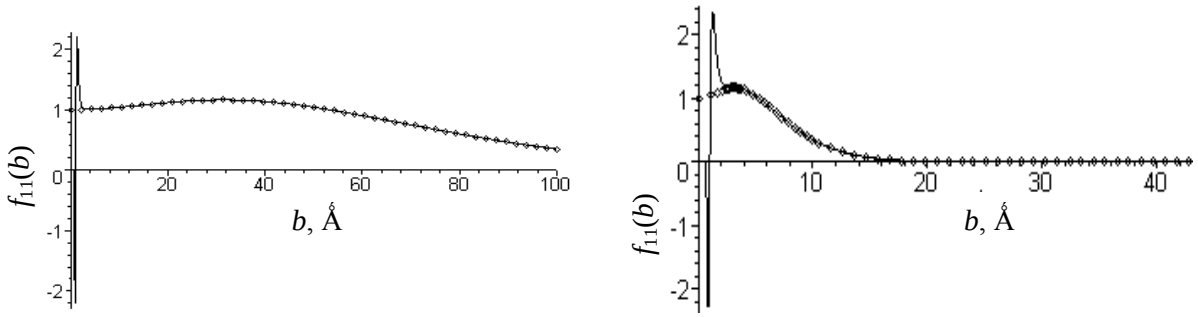

Fig. 4. The resonance function for the dipole-dipole interaction of the CO-CO system for the transition frequencies of 1 cm^{-1} (a) and 10 cm^{-1} (b): °° - "old" resonance function, __ - "new" resonance function.

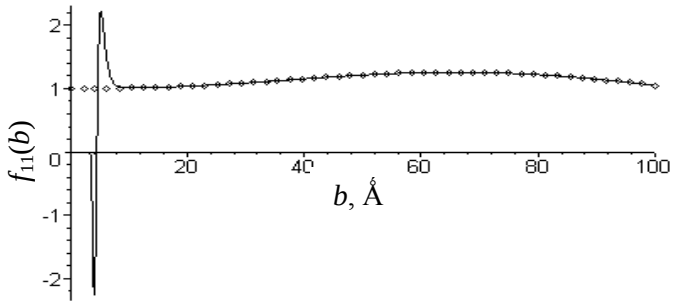

Fig. 5. The resonance function for the dipole-quadrupole interaction of the HF-N_2 system when the transition frequency equals 1 cm^{-1}: °° - "old" resonance function, __ - "new" resonance function.

The "new" resonance functions give most contribution to the interruption function when the frequency is small (non-adiabatic case). At frequencies higher then 10 cm^{-1} the resonance function goes to zero (adiabatic case) and the second-order contribution to the interruption function is minimal.

Chapter III

Broadening and shifting coefficients calculations of ozone spectral lines calculated by semi-classical and semi-empirical methods

The knowledge of collisional parameters of ozone spectral lines is necessary for studies of physical and chemical processes in the troposphere and stratosphere as well as for studies of solar radiation absorption.

III.1. Calculation of O_3-N_2 and O_3-O_2 line widths

Line-broadening coefficients for the most important for atmospheric application cases of O_3-N_2 and O_3-O_2 broadening were calculated by the semi-classical RB formalism with exact trajectories and the semi-empirical method. More details on these calculations can be found in Appendix B [6*].

Figures 6 and 7 show the comparison of calculated values with experimental data for the Q-, *P*- and *R*-branch of the $\nu_1+\nu_3$ band. To separate the broadening coefficients with the same *J* values but different K_a values we selected a specific variable $J+0.05(K_a-1)$ for the abscissa.

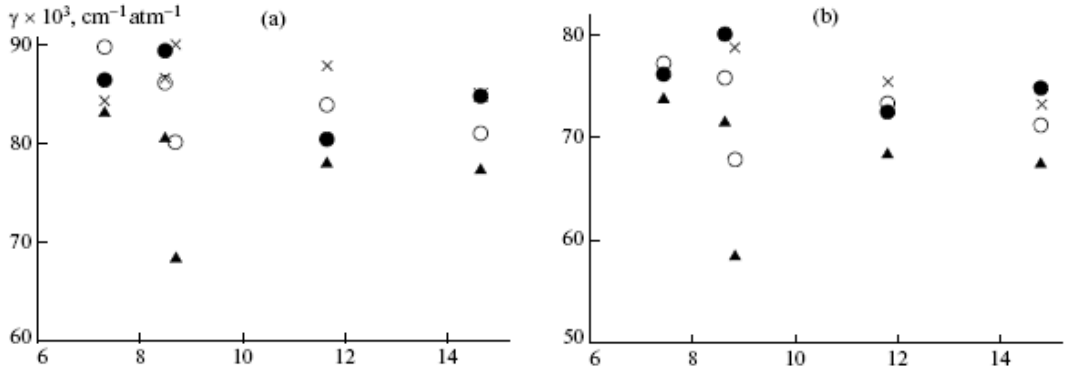

Fig. 6. Calculated by the RB formalism with (triangles) parabolic [27] and with (full circles) exact trajectories and by (crosses) the semi-empirical method [21] and (open circles) experimental data [27, 28] line broadening coefficients for lines of the *Q*-branch of the ozone $\nu_1+\nu_3$ vibrational band in nitrogen (a) and oxygen (b) atmosphere.

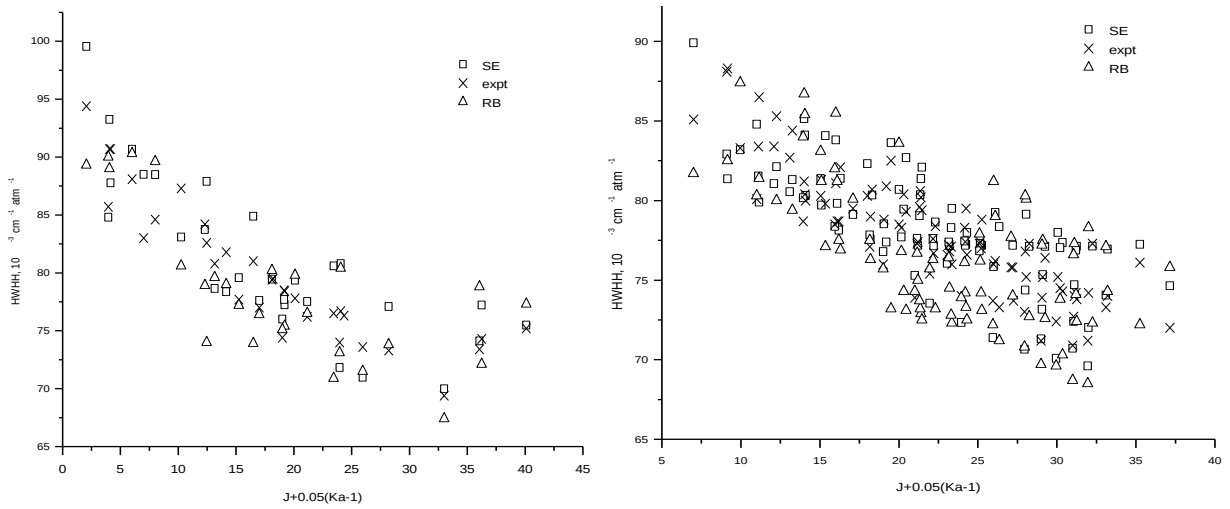

Fig. 7. Calculated by the RB formalism with parabolic trajectories [27] and by the semi-empirical method [21] and experimental [27, 28] line broadening coefficients for: (a) lines of the *R*-branch of the O_3-N_2 and (b) lines of the *P*-branch of the O_3-O_2 of the $\nu_1+\nu_3$ band.

As the line broadening coefficients depend weakly on the vibrational quantum numbers, the semi-empirical model parameters c_1 and c_2 obtained for one vibrational band can be used for calculations of these coefficients for other bands. In contrast with the highly polar water vapour molecule, the parameters c_1 and c_2 for O_3 molecule demonstrate an observable dependence on the rotational quantum number values J and a weaker dependence on the type of branch. Therefore, the fitting parameters were determined for three intervals of rotational quantum numbers J – small, middle and high values. The parameter c_1 varies only slightly when passing from low to middle J and more significantly for high J and is responsible for correction of the error induced by the interruption procedure. The parameter c_2 includes the vibrational dependence which is really more complex.

As can be seen from Figures 6 and 7, the separate fitting to the data of only the *R*-branch mostly improves the computation quality. For the O_3-N_2 system, the initial rms deviation of 2.33×10^{-3} $cm^{-1}atm^{-1}$ (simultaneous fitting to the data for the *P* and *R*-branches) for the whole set of studied lines decreases down to 2.29×10^{-3} $cm^{-1}atm^{-1}$ (separate fitting for the *P* and *R*-branches). This improvement is insignificant, and the dependence of the fitting parameters on the type of branch can be considered as negligibly weak.

From these figures we can make a conclusion that values of line broadening coefficients received by using RB formalism with exact trajectories and semi-empirical approach are in a good agreement with data of experiments (see Appendix B and [6*]). So, the modification of the semiclassical RB formalism with exact trajectories requires long time for calculations due to numerical integration, but this modification is justified. Using of fitting parameters of semi-

empirical method obtained for the $\nu_1+\nu_3$ band allows calculating the broadening coefficients for lines of other ozone vibrational bands.

III.2. Calculation of vibrational shifts of O_3-N_2 lines

The goal of this study was to check the importance of vibrational dependence of classical trajectories for a molecular system of practical interest, and not for a very particular system as did Ma and co-authors [20]. The initial project consisted, first, in calculation of purely vibrational O_3-N_2 line shifts by the RB formalism with vibrationaly-dependent exact classical trajectories; then the rotational contributions (defined by S_2 terms) should be added. By the lack of time, only the first part has been realized and is shortly described here.

We started with the vibration-dependent contribution S_1 for exact trajectories proposed by Ma et al. [20]:

$$S_1(b) = \frac{2r_{c,(f)}}{\hbar v}\int_1^{+\infty} x\,dx \frac{\left[\Delta V_{iso,(f)}(xr_{c,(f)})\right]}{\left\{x^2 - 1 + \frac{2V_{iso,(f)}(r_{c,(f)})}{mv^2} - \frac{2x^2 V_{iso,(f)}(xr_{c,(f)})}{mv^2}\right\}^{\frac{1}{2}}} -$$

$$- \frac{2r_{c,(i)}}{\hbar v}\int_1^{+\infty} x\,dx \frac{\left[\Delta V_{iso,(i)}(xr_{c,(i)})\right]}{\left\{x^2 - 1 + \frac{2V_{iso,(i)}(r_{c,(i)})}{mv^2} - \frac{2x^2 V_{iso,(i)}(xr_{c,(i)})}{mv^2}\right\}^{\frac{1}{2}}} \qquad (3.1)$$

where $\Delta V_{iso,(f)}(r) = \langle f|\Delta V_{iso}(r,\xi)|f\rangle$, $\Delta V_{iso,(i)}(r) = \langle i|\Delta V_{iso}(r,\xi)|i\rangle$, $V_{iso,(f)}(r) = \langle f|V_{iso}(r,\xi)|f\rangle$ and $V_{iso,(i)}(r) = \langle i|V_{iso}(r,\xi)|i\rangle$; ξ is the normalized vibrational coordinate defined by $\xi \equiv (r - r_e)/r_e$, where r is the vibrational displacement and r_e the equilibrium displacement, V_{iso} is the isotropic part of the interaction potential, ΔV_{iso} is vibrationally dependent part of potential.

From Eq. (3.1) it is seen that $S_{1,(i)}$ and $S_{1,(f)}$ are calculated with different minimal r_c values: $r_{c,(i)}$ and $r_{c,(f)}$. In order to define these values the long-range isotopic potential was approximated by the induction and dispersion terms, as described in Sec. I.3, which provide the vibrational dependence of trajectories via the dipole moment and polarizability of the active molecule.

Since the determination of $r_{c,(i)}$, $r_{c,(f)}$ requires also the short-range part of the isotropic potential (for which the vibrational dependence is not available), we used the repulsion term in the form

$$V_{iso}^{short-range}(r) = \frac{4\varepsilon\sigma^{12}}{r^{12}} \ , \tag{3.2}$$

where ε and σ are the usual Lennard-Jones parameters.

The interaction potentials in the final f ($\nu_1+\nu_3$) and initial (ground) i states are shown in Figure 8. The vibrationally dependent interaction potentials were calculated with new values of Lennard–Jones potential parameters described below. From this figure it can be seen that the values of the potential in the f and i states slightly differ from each other – about $0.5*10^{-15}$ cm^{-1}. Figure 9 presents these two curves in comparison with the standard Lennard–Jones potential (ε=150K and σ=3.93 Å) [29] used in the literature for O_3-N_2. Their differ significantly, especially in the potential well region.

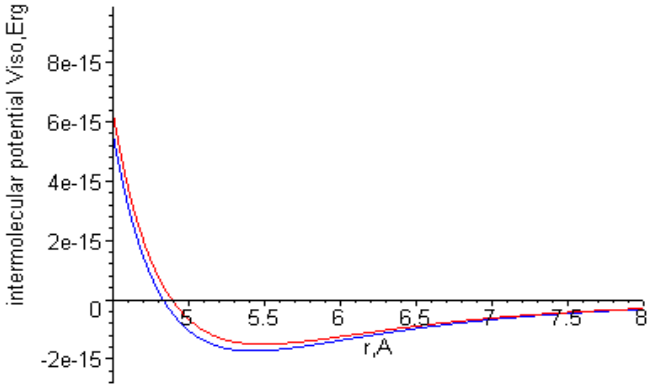

Fig. 8. The interaction potential V_{iso} in the initial ground (red line) and final $\nu_1+\nu_3$ (blue line) states.

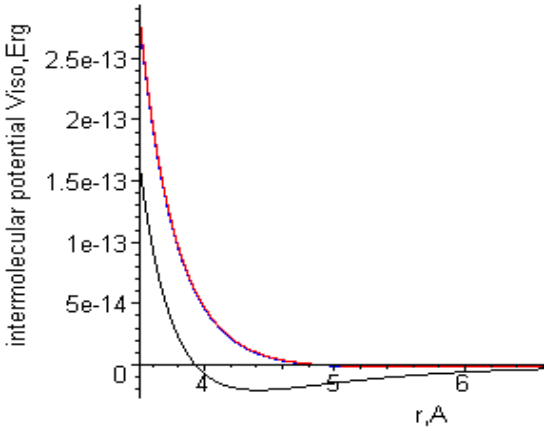

Fig. 9. The vibrationally dependent interaction potential V_{iso} in the initial ground and final $\nu_1+\nu_3$ states and the standard Lennard-Jones potential (ε=150K and σ=3.93Å) from the literature. $V_{iso(i)}$ – red line, $V_{iso(f)}$ – blue line, $V_{(LJ)}$ – black line.

To obtain new, more appropriate, Lennard–Jones parameters for the vibrationally dependent isotropic potential, we supposed the equivalence between the induction and dispersion terms in r^{-6} and the attractive part of the Lennard–Jones potential (ε will fixed at 150K for O_3-N_2 and the same for O_3-O_2)

$$\frac{\left(\mu_1^2 + \frac{3}{2}\frac{I_1 I_2}{I_1 + I_2}\alpha_1\right)\alpha_2}{r^6} \sim \frac{4\varepsilon\sigma^6}{r^6}, \qquad (3.3)$$

Which leads to σ=3.1949 Å for the O_3-N_2 system and σ=3.0637 Å for the O_3-O_2 system. The values of σ for other vibrational bands are presented in Table I. The O_3-N_2 isotropic potentials for the initial (ground) and final ($\nu_1+\nu_3$) states (σ=3.1949 Å) are presented in Figure 10.

Table I. The values of Lennard–Jones parameter σ for the O_3-N_2 and O_3-O_2 systems (ε=150K).

Band	σ, Å O_3-N_2	σ, Å O_3-O_2
$\nu_1+\nu_3$	3.1949	3.0637
$2\nu_1$	3.1670	3.0368
$2\nu_3$	3.2218	3.0896
ν_1	3.1624	3.0325
ν_3	3.1907	3.0598

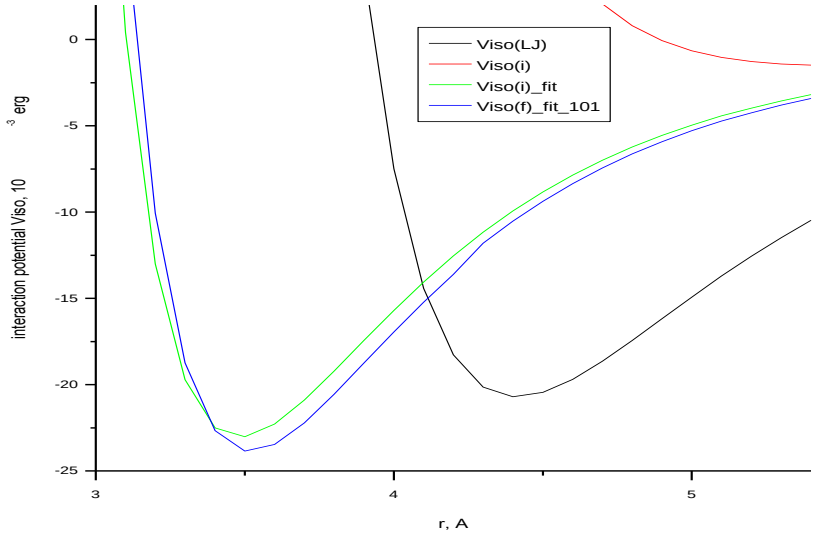

Fig. 10. V_{iso}(LJ) – the standard Lennard-Jones potential (ε=150K and σ=3.93Å), V_{iso}(i) – vibrationally dependent potential for the initial state with the standard values of σ and ε, Viso(i)_fit, and Viso(f)_fit_101 – the vibrationally dependent potential in the initial and final ($\nu_1+\nu_3$) states with ε=150K and σ=3.1949 Å.

The relation between r_c and b

$$b^2 = r_c^2 \left\{1 - V_{iso}^*(r_c)\right\}$$

becomes therefore

$$b^2 = r_{c,(i/f)}^2 - \frac{8\varepsilon\sigma^{12}}{mv^2}\frac{1}{r_{c,(i/f)}^{10}} + \frac{2\alpha_2\left(\mu_{1,(i/f)}^2 + \frac{3}{2}\frac{I_1 I_2}{I_1 + I_2}\alpha_{1,(i/f)}\right)}{mv^2}\frac{1}{r_{c,(i/f)}^4} \qquad (3.4)$$

Eq. (3.1), in its turn, reads

$$S_1(r_c) = \frac{1}{\hbar v}\int_1^{x_{\max}} \frac{-\alpha_2\left(\mu_{1,(f)}^2 + \frac{3}{2}\frac{I_1 I_2}{I_1 + I_2}\alpha_{1,(f)}\right)dx}{r_{c,(f)}^5 x^6\sqrt{x - 1 + V_{iso}^*(xr_{c,(f)})}} - \frac{1}{\hbar v}\int_1^{x_{\max}} \frac{-\alpha_2\left(\mu_{1,(i)}^2 + \frac{3}{2}\frac{I_1 I_2}{I_1 + I_2}\alpha_{1,(i)}\right)dx}{r_{c,(i)}^5 x^6\sqrt{x - 1 + V_{iso}^*(xr_{c,(i)})}} \qquad (3.5)$$

where $\mu_{1,(f)}$ is the dipole moment and $\alpha_{1,(f)}$ is the polarizability of the radiating molecule in high excited state *f*.

Table II presents a comparison of the line-shifting coefficients in the $\nu_1+\nu_3$ band of the O_3-N_2 and O_3-O_2 systems obtained by the RB formalism with exact trajectories taking into account the vibrational dependence of the isotropic interaction potential with the semi-empirically-calculated [21] and the experimental ones [30]. In our RBE-calculations of the purely vibrational line shifts we first took into account the vibrational dependence of the isotropic interaction potential with the same, vibrationally independent, trajectory for the initial and final states (RBE calc.1 in Table II), then, for this V_{iso}, we considered two different trajectories for the *i* and *f* states (RB calc.2 in Table II). The experimental values of the vibrational shifts for the lines with high *J* (and low K_a) values give an estimation for the asymptotic behaviour which should be observed for purely vibrational shifts.

From Table II it can be seen that the purely vibrational line shift calculation with vibrationally dependent isotropic potential and two different trajectories for *i* and *f* states differ noticeably from the results with one and the same trajectories.

Table II. Comparison of the calculated and experimental ozone line-shifting coefficients (in $cm^{-1}atm^{-1}$) for the $\nu_1+\nu_3$ band.

O_3-N_2									
J′	K'_a	K'_c	J″	K''_a	K''_c	SE calc. [21] (vib-rotational),	expt. [30] (vib-rotational)	RBE calc.1 (vibrational)	RBE calc.2 (vibrational)
31	1	30	32	1	31	- 2.85	- 3.8	- 3.86	- 2.1
O_3-O_2									
J′	K'_a	K'_c	J″	K''_a	K''_c	SE calc. [21] (vib-rotational)	expt. [30] (vib-rotational)	RBE calc.1 (vibrational)	RBE calc.2 (vibrational)
27	0	27	26	0	26	- 4.53	- 3.0	- 3.17	not calculated

In this study a model vibrationally dependent isotropic potential was proposed of vibrationally dependent line shifts of the O_3-N_2 and O_3-O_2 systems. The parameters of this were determined for various vibrational bands of O_3-N_2. It is shown that taking into consideration min and max of the vibrational dependence of classical trajectories has an influence on calculations of vibrational line shifts. Consequently, in order to improve calculations it is necessary to examine the vibrational dependence of trajectories for the considered molecular pair.

Since in our calculations we don't take into account the rotational dependence of ozone line-shifting coefficients therefore we do asymptotic comparison for our data. The addition of rovibrational contributions to line-shifting coefficients and comparison ones with other calculated data [31] will be in future.

Chapter IV

Calculation of broadening and shifting coefficients of water vapour lines by semi-empirical method

An accurate knowledge of the water vapour line pressure broadening and shifting coefficients induced by N_2, O_2, H_2O and other atmospheric gases is of interest for many atmospheric applications including models of the propagation of laser radiation along vertical and slanted paths [32].

As mentioned above, the details of the semi-empirical approach are given in Ref. [21]. The main feature of the semi-empirical approach applied to the H_2O molecule is the use of a complete set of high-accuracy vibration-rotation dipole transition moments calculated for all possible transitions using the wave functions determined from variational nuclear-motion calculations and an *ab initio* dipole moment surface (DMS). This approach explicitly takes into account all scattering channels induced by collisions. Results of these calculations clearly demonstrate an improved agreement between observed and calculated parameters for both line widths and line shifts and, in principle, extends the range of applicability of the semi-empirical method up to the dissociation limit [33]. However, it should be kept in mind that the method of effective Hamiltonians (EH) traditionally used for determination of vibrational energies and wave functions of the active molecule is based on perturbation theory expansions which have poor convergence for highly excited states. In addition, the parameters of these effective Hamiltonians are usually extracted from experimental spectra, so that massive calculations are not possible. At the same time, variational methods do not suffer from this problem and also take into account all intra-molecular effects.

In our work we used energy levels and dipole transition moments from the BT2 (Barber and Tennyson) line list [34]. This line list was constructed using the DVR3D nuclear motion suite [35], the semi-empirical Potential Energy Surfaces of Shirin et al. [36] and Schwenke and Partridge's Dipole Moment Surface [37]. The BT2 line list includes all transitions between rotation-vibration states of water up to 30000 cm^{-1} above the ground state and with rotational excitation up to J = 50. This gives in total 221,000 states and $5.08*10^8$ transitions. Further information can be found in the original publication [34]. The H_2O molecular constants required for calculations (mean dipole moments in the ground and excited vibrational states, components of quadrupole moments, and dipole polarizability) were taken from Refs [38-40], respectively. All calculations were made for the room temperature T=297 K. The parameters c_1 and c_2 were fitted to the measured N_2- broadening coefficients of the $2\nu_1+2\nu_2+\nu_3$ band c_1=1.08, c_2=0.11 and then were used for all subsequent calculations of both N_2- broadening and shifting.

IV.1. Calculation of line-broadening and shifting coefficients of water vapour lines induced by N_2 and O_2 pressure

For the line shift calculation the "effective" dipole polarizability in the upper vibrational state was used as one more additional fitting parameter; its values obtained for the studied bands are listed in Table III.

Table III. "Effective" dipole polarizability in the upper vibrational states.

Band	Polarizability, Å^3	Band	Polarizability, Å^3
ν_2	1.496	$3\nu_1+\nu_2+\nu_3$	1.631
ν_3	1.502	$3\nu_1+2\nu_2+\nu_3$	1.640
ν_1	1.510	$4\nu_1+\nu_3$	1.641
$\nu_1+\nu_2+\nu_3$	1.561	$4\nu_1+\nu_2+\nu_3$	1.646
$\nu_1+2\nu_3$	1.606	$5\nu_1+\nu_3$	1.655
$2\nu_1+\nu_3$	1.572	$5\nu_1+\nu_2+\nu_3$	1.690
$2\nu_1+2\nu_2+\nu_3$	1.601	$6\nu_1+\nu_3$	1.682
$3\nu_1+\nu_3$	1.609	$7\nu_1+\nu_3$	1.710
$\nu_1+3\nu_3$	1.660		

Our calculated values were compared with both experimental data and calculations based on the effective Hamiltonian of Watson (see Figs. 1-2 and Table III of Appendix C [2*]). It can be seen that half-widths calculated using variational wave functions agree reasonably well with those obtained using the standard approach of perturbative wave functions from the Watson's effective Hamiltonian and an effective dipole moment operator. For most lines the differences in half-widths do not exceed 10%. However, the differences are larger for the line shift coefficients: usually about common 20% but up to 35% in some cases. This demonstrates that the shift coefficients are more sensitive to different intra-molecular interactions.

We have also studied the problem of drastic disagreement between the line width data included in HITRAN database and recent experimental values obtained by a Franco-Belgian group with a Fourier-transform spectrometer (FTS) in the region 13000-26000 cm^{-1}. To understand the possible origins of this problem we compared our calculated line width values

with the experimental ones for the $3\nu_1+\nu_3$ band (Fig. 11). This figure shows that the experimental values obtained in Refs [2] and [41, 42] differ strongly. The discrepancies between the measurements reach 0.02 $cm^{-1}atm^{-1}$ (25%). Our calculations agree well with the experimental values of [2], with a root mean square (RMS) of 0.0056 $cm^{-1}atm^{-1}$, and agree poorly with the FTS experiment [41] (RMS = 0.011 $cm^{-1}atm^{-1}$ for the same lines).

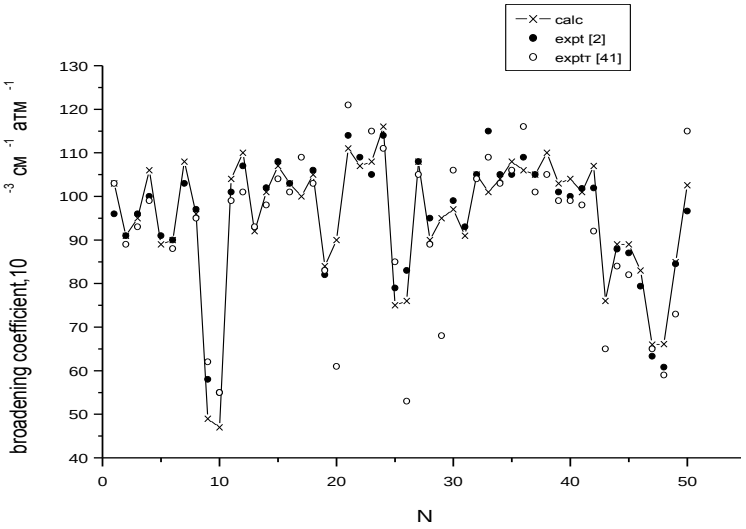

Fig. 11. Comparison of our calculated and available experimental broadening coefficients for lines of the $3\nu_1+\nu_3$ band. *N* is the number of the vibration-rotation transitions according to increasing of frequency and correspond to the numbering given in Ref. [43].

An analysis of the spectral intervals for which Refs. [41, 42] give large broadening coefficients shows that they are characterized by blended lines [2*]. For such cases the fitting of a single profile to blended lines leads to very significant overestimation of the broadening.

For the line shifting coefficients, the situation is similar (see Fig. 12 of Appendix C [2*]). The experimental data of Ref. [2] agree very well with our calculations (RMS = 0.00056 $cm^{-1}atm^{-1}$). The agreement of experimental data [41, 42] with our calculations is much worse (RMS = 0.0009 $cm^{-1}atm^{-1}$). For some lines the shift coefficients of Refs [41, 42] are more than twice greater than those of Ref. [2], or even differ in sign.

We find and noted in our paper [2*] (Appendix C) that the largest disagreement between the BT2 and EH calculations takes place for high bending vibrations. For example, the $3\nu_1+\nu_3$ band involves no excitation of bending vibrations and the EH method works well; RMS are the same for calculations using EH or variational wave functions. In contrast, for the $2\nu_1+2\nu_2+\nu_3$ band which involves two quanta of bending excitation, our method gives better agreement with the experimental data in Ref. [2]. For example, the RMS of line shifts is 0.0005 $cm^{-1}atm^{-1}$ for the complex RB calculations [44] and 0.0004 $cm^{-1}atm^{-1}$ for our calculations. The decreasing line width in these bands is influenced by the centrifugal distortion – the so-called Δk effect [45], which leads to a strong change in the energy structure in high bending states.

We made calculations using this method for more than 200 000 transitions, corresponding to the most intense lines, for the H_2O-N_2 and H_2O-O_2 colliding systems. Line broadening and shifting coefficients, as well as their temperature exponents, have been calculated. The results of these calculations are available via the "ATMOS" Information System (http://saga.atmos.iao.ru) and spectroscopic data bank GEISA (http://ara.lmd.polytechnique.fr/htdocs-public/ref_for_geslines_2008.html, details of changes since the 2003 edition of GEISA).

IV.2. Calculation of self-broadening and self-shifting coefficients of water vapour

In the self-broadening case the main contribution to the line widths is given by the dipole-dipole interaction. We also take into account the higher-order electrostatic (dipole-quadrupole, and quadrupole-dipole) interactions as well as polarization (induction and dispersion) interactions.

We performed the calculations of self-broadening coefficients of water vapor lines for the $3\nu_1+\nu_3$, $2\nu_1+2\nu_2+\nu_3$ and ν_3 vibration-rotation bands, experimentally studied in [1, 4* Appendix D]. All the calculations were made for the room temperature T=297 K. Fig. 12 presents the calculated and experimental self-broadening coefficients for the $3\nu_1+\nu_3$ band (*N* is the number of the vibration-rotation transitions according to increasing of frequency). It is seen that the calculations are in satisfactory agreement with experiment. The self-broadening coefficients of water vapor lines, calculated with the same set of the fitting parameters for all bands agree reasonably experimental values.

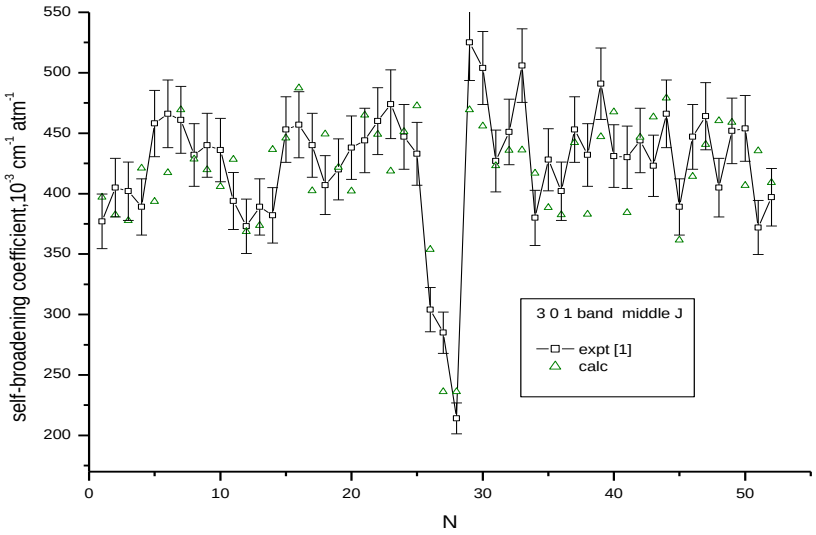

Fig. 12. Calculated and experimental [1] water self-broadening coefficients for the band $3\nu_1+\nu_3$ (middle *J*). *N* is the number of the vibration-rotation transition according to increasing of frequency.

In Fig. 12 in order to analyze the self broadening more carefully we separate the lines in three groups with low (J < 4), middle (3 < J < 7) and high (J > 6) rotational quantum numbers. After that, the model parameters were fitted for each group of lines. The results of fitting are presented in Table IV. This table shows that the c_1 coefficient depends on the quantum number J value: $c1$=1.31-0.042*J.

Table IV. Mean root-square deviation (MRSD) in the case of separating the calculation with respect to J values and varying the model parameters c_1, c_2 and gas kinetic diameter R_0.

a) – present method; b) – Watson Hamiltonian

a)

Rotational quantum number J	(**3 0 1**) band		(**2 2 1**) band	
	MRSD γ		MRSD γ	
low (J<4)	R_0=7.76 c_1=1.23 c_2=0.08	R_0=10.0 c_1=1.23 c_2=0.08	R_0=7.76 c_1=1.23 c_2=0.08	R_0=10.0 c_1=1.23 c_2=0.08
	0.0109346	0.006728273	0.0113214	0.008595
middle (3<J<8)	R_0=7.76 c_1=1.23 c_2=0.08	R_0=7.76 c_1=1.1 c_2=0.1	R_0=7.76 c_1=1.23 c_2=0.08	R_0=7.76 c_1=1.1 c_2=0.1
	0.005704511	0.005	0.023121214	0.021936396
high (J>7)	R_0=7.76 c_1=1.23 c_2=0.08	R_0=7.76 c_1=0.9 c_2=0.08	R_0=7.76 c_1=1.23 c_2=0.08	R_0=7.76 c_1=0.9 c_2=0.08
	0.0230145	0.0152971	0.049289817	0.032120113

b)

Rotational quantum number J	(**3 0 1**) band		(**2 2 1**) band	
	MRSD γ		MRSD γ	
low (J<4)	R_0=7.76 c_1=1.23 c_2=0.08	R_0=10.0 c_1=1.23 c_2=0.08	R_0=7.76 c_1=1.23 c_2=0.08	R_0=10.0 c_1=1.23 c_2=0.08
	0.0064649	0.0104901	0.0110736	0.008928
middle (3<J<8)	R_0=7.76 c_1=1.23 c_2=0.08	R_0=7.76 c_1=1.1 c_2=0.1	R_0=7.76 c_1=1.23 c_2=0.08	R_0=7.76 c_1=1.1 c_2=0.1
	0.0056495	0.0047727	0.0244309	0.0228648
high (J>7)	R_0=7.76 c_1=1.23 c_2=0.08	R_0=7.76 c_1=0.9 c_2=0.08	R_0=7.76 c$_1$=1.23 c_2=0.08	R_0=7.76 c_1=0.9 c_2=0.08
	0.0247585	0.0157944	0.0675662	0.0417901

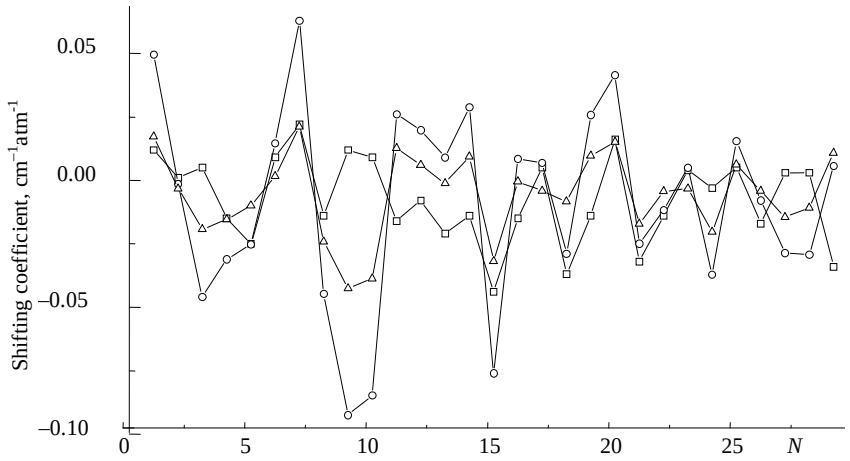

Fig. 13. Calculated and experimental [1] self-shifting coefficients for medium J values for the band $3\nu_1+\nu_3$. N is the number of the vibration-rotation transitions according to increasing of frequency.

The dependence of water line broadening coefficients on the "good" quantum numbers (angular momentum and symmetry of the upper and lower levels) has been analyzed for the rotational quantum numbers up to J=50. Trends were investigated separately for the P-, Q-, and R-branch transitions for the atmospherically important water isotopologues $H_2{}^{17}O$, $H_2{}^{18}O$, $HD^{16}O$. Two different methods were used: averaging the broadening coefficients from HITRAN-2008 for small J values and averaging of data calculated by the semi-empirical method for higher J. The resulting air-broadening coefficients allow calculation of water vapour spectra with millions of weak lines with an accuracy reasonable for many applications, for example, estimation of the sun radiation with low resolution. These results have been presented in [7*] (Appendix E).

Chapter V

Influence of the water vapour line interference on the atmospheric transmission of near-IR radiation

The collision-induced interference of spectral lines in vibrational-rotational spectra of molecular gases is the object of numerous investigations [46-48]. This interference influences absorption, emission, and Raman spectra of dense gases, absorption in atmospheric windows and microwindows, as well as line wings. In particular, when solving problems associated with laser sensing, the influence of interference on spectroscopic parameters of spectral lines should be carefully examined. The most important cases for atmospheric applications are given by H_2O, CO_2, CH_4 (and some other molecules) in a mixture with nitrogen and oxygen at temperatures 200–300 K.

A relation of intramolecular resonances (such as Coriolis, Fermi, and Darling–Dennison resonances) with the line interference was established in Ref. [48]. A nonlinear pressure dependence of the line shift and a deviation of the line shape from the Lorentz profile were also observed. It was found that in the range of 0.8 μm the contribution of the line interference in the atmospheric extinction of radiation can reach several percents. That is why corrections for the line interference should obviously be taken into account in analysis of high-resolution atmospheric spectra.

We carried out theoretical studies of the IR line interference in spectra of water vapour and estimated its influence on the atmospheric transmission for slant and vertical atmospheric paths for summer and winter conditions of the atmosphere model for middle latitudes [49, 50].

V.1. Basic equations for a line profile accounting for line interference

The full description of a line profile taking into account line interference in presented in our paper [3*] (Appendix F) so that only main formulae are briefly reminded here.

In the impact approximation, the absorption coefficient for overlapping lines can be written as [46, 47]

$$k(\omega) = \frac{n_a}{\pi} \operatorname{Im}\left\{ \sum_{m,n} \mu_m << m \left| \left[\omega \times \mathbf{1} - \omega_0 - i\mathbf{W} \right]^{-1} \right| n >> \mu_n \rho_n \right\}, \qquad (5.1)$$

where n_a is the density of absorbing molecules, subscripts m and n enumerate the lines and include all the necessary quantum numbers of the initial and final states related to the transition moment μ , and ρ_n is the population of the lower state of the transition n; the matrix ω_0 is diagonal: $\left\langle\left\langle m\left|\omega_0\right|n\right\rangle\right\rangle = \omega_m^0 \delta_{mn}$, where ω_m^0 is the proper frequency of free active molecule; W is the relaxation matrix. The real and imaginary parts of the diagonal elements of W determine the half-width γ_m^0 and the shift δ_m^0 of isolated spectral lines (in the absence of overlapping).

In order to calculate the line shape parameters and the absorption coefficient it is necessary to determine the resolvent matrix $\left[\omega \times \mathbf{1} - \omega_0 - i\mathbf{W}\right]^{-1}$, for example, using the diagonalisation of the non-Hermitian matrix $\omega_0 + i\mathbf{W}$. Then we can write the absorption coefficient as a sum of Lorentzian profiles. Since at atmosphere pressure the Doppler broadening is responsible for a significant fraction, the joint action of the collisional and Doppler broadening is taken into account via the convolution of the Doppler spectral distribution $D(\omega)$ with the spectral function $k(\omega)$ of Eq. (5.1).

The absorption for a slant path is determined by

$$K(h) = \int_0^h \left(1 - \mathrm{e}^{-k(\omega)P(h)h}\right) dh \tag{5.2}$$

where $k(\omega)$ is the profile of the corresponding line, h is the altitude, $P(h)$ is the pressure of the air, which depends on the altitude and the tilt angle of the path [48].

V.2. Influence of H_2O line interference on the atmospheric transmission for horizontal, vertical, and slant atmospheric paths

Our calculations have been performed for the spectral range 12412–12415 cm^{-1}, which includes two lines centred at 12414.2027 and 12413.9720 cm^{-1}. These lines correspond to the transitions 634←541 of the $8\nu_2$ band and 652←541 of the $3\nu_1 + \nu_2$ band considered here. The cross-relaxation parameters W_{kl}, half-widths γ_k, and shift coefficients δ_k necessary for calculations of the absorption coefficients were calculated for these two lines in the case of broadening by nitrogen and oxygen in the temperature range 200–330 K. The data are summarized in Table I [3*] (Appendix F) according to the following equation:

$$X(\text{air}) = 0.79X(\text{N}_2) + 0.21X(\text{O}_2), \tag{5.3}$$

where X is any of the parameters γ_k, δ_k, Y_k, W_{kl} .

For the resonance lines mentioned above and involved in the so-called HEL (Highly excited local) resonance [51] caused by the abnormally strong centrifugal effect in H_2O, the strong effect of the interference is observed: the coefficients Y_k are about 0.02 $cm^{-1}atm^{-1}$ at room temperature.

In Ref. [48] the calculations were performed for a horizontal path at a path length of l = 100–1000 m, temperature of 297 K, and air pressure of 760 Torr, and only the absorption by water vapour was taken into account. In the considered case the influence of the interference was found to be low: the highest addition is 3% at 12414.07 cm^{-1}. It was concluded that the line interference leads to an increased absorption in the atmospheric microwindows.

The calculation of the transmission coefficient for a slant path was also made, with the atmospheric models of mid-latitudinal summer and winter [49, 50]. In this calculation, it was necessary to take into account the dependences of the line profile parameters and the cross-relaxation parameters on temperature, pressure, and water vapour concentration, whereas the dependences, in their turn, are function of the zenith angle (Table V). The calculations were performed using the profile from Ref. [47] taking into account line interference and Doppler broadening.

Table V. Pressure, temperature, and concentration of water vapour in the range 0–10000 m [49, 50, 3*]

h (m)	Summer conditions			Winter conditions		
	P (atm)	T (K)	n (atm)	P (atm)	T (K)	n (atm)
0	1.013	292	0.0205	1.018	272	0.0077
1000	0.9020	288	0.0155	0.8973	270	0.0059
2000	0.8020	283	0.0111	0.7897	267	0.0040
3000	0.7100	278	0.0077	0.6938	263	0.0029
4000	0.6280	272	0.0052	0.6081	257	0.0019
5000	0.5540	266	0.0036	0.5313	251	0.0012
6000	0.4870	260	0.0021	0.4627	244	0.00073
7000	0.4260	253	0.0012	0.4016	237	0.00042
8000	0.3720	246	0.00084	0.3473	231	0.00014
9000	0.3240	239	0.00052	0.2992	224	0.000071
10000	0.2810	233	0.00031	0.2568	220	0.000038

For a slant path and a vertical path as its particular case, we considered the influence of the interference on the water vapour absorption in the atmosphere and analyzed how the absorption varies under winter and summer conditions.

One can see from the frequency dependence of the absorption in the range 12414–12414.2 cm^{-1} (Fig. 14) that under summer conditions the interference contributes 0.5%, while under

winter conditions the influence of interference is about 1.5%. If the shift is taken into account, the lines shift toward lower frequencies. Simultaneous consideration of the line interference and of the shift gives corrections of about 7% for winter and about 1% for summer conditions. As the zenith angle increases (Figs. 15a and 15b), the influence of the interference halves. For a path tilt angle of 75°, the microwindow disappears (Fig. 15c). In the line wing, the neglect of the interference leads to a larger error than the neglect of the shift does (Figs. 16a–16b).

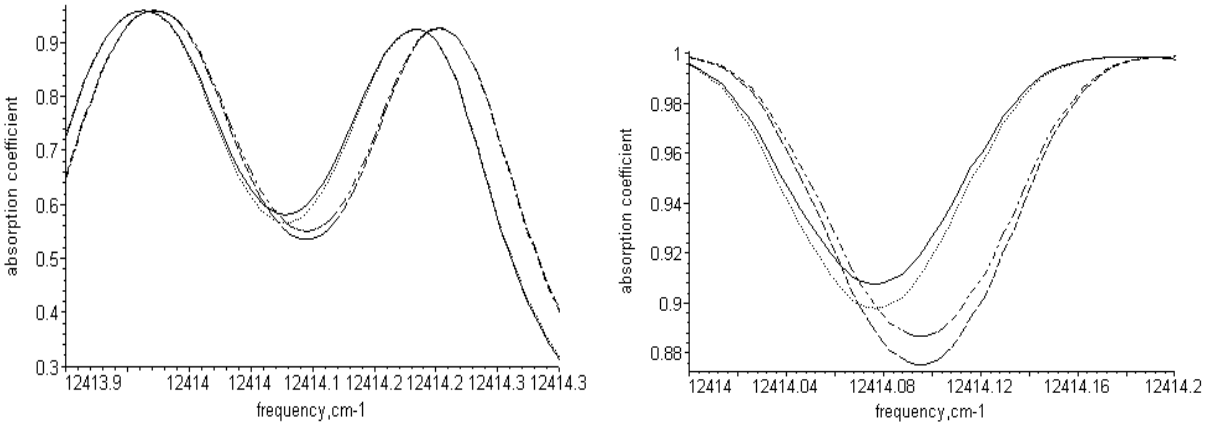

(a) (b)

Fig. 14. Frequency dependence of the absorption for a slant atmospheric path (at an angle of 30°): (a) (winter conditions) frequency range 12413.9–12414.3 cm^{-1}, (b) (summer conditions) microwindow range 12414–12414.2cm^{-1}; (dotted curve) absorption with regard for interference and shift, (solid curve) absorption with regard for shift but neglecting interference, (dashed curve) absorption with regard for interference but with zero shift, (dot-and-dash curve) absorption with neglected interference and with zero shift.

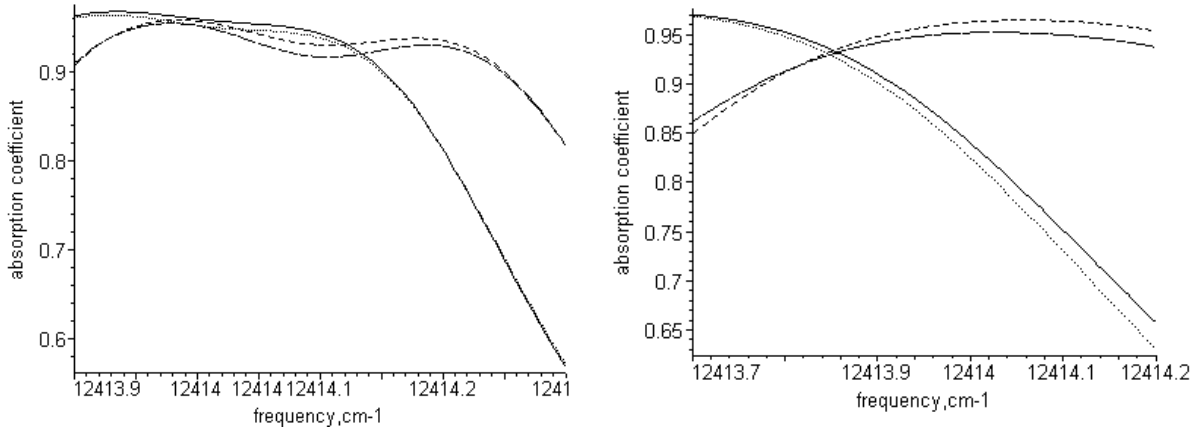

(a) (b)

Fig. 15. Frequency dependence of absorption for a slant atmospheric path: (a) (at an angle of 60°, winter conditions) microwindow range 12413.9–12414.3 cm^{-1}, (b) (at an angle of 75°, summer conditions) microwindow range 12413.7–12414.2 cm^{-1}. Designations are the same as in Fig. 14.

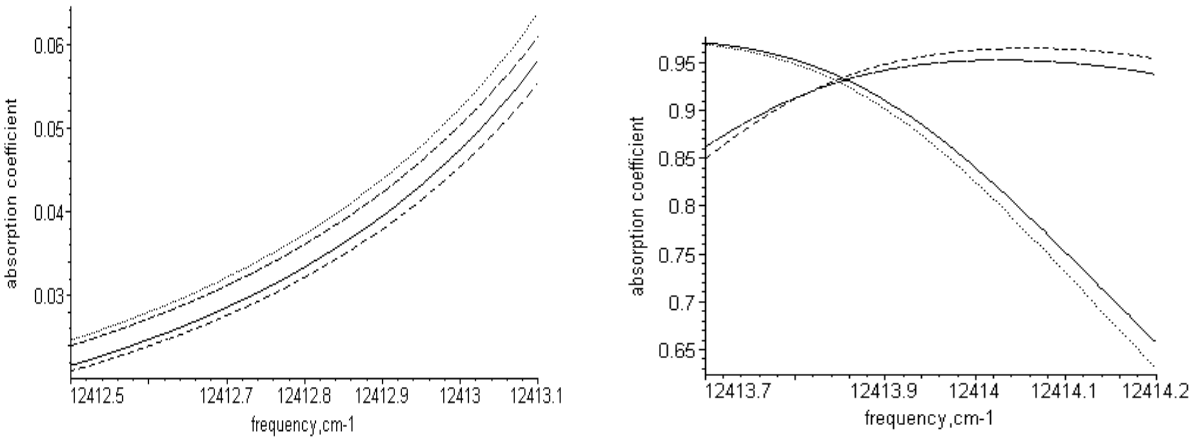

(a) (b)

Fig. 16. Frequency dependence of absorption for a slant atmospheric path in the microwindow range 12412,5 – 12413,1 cm^{-1} (summer conditions): (a) at an angle of 30°, (b) at an angle of 75°. Designations are the same as in Fig. 14.

In conclusion, it should be noted that our calculations demonstrate that the interference of H_2O lines contributes significantly to the atmospheric extinction of radiation, leads to the disappearance of atmospheric microwindows and should be taken into account in calculations of the transmission of laser radiation.

Basic results

1. Using the generalised Euler series transformation allowing obtaining the resonance functions necessary for calculations of half-widths and shifts of molecular spectral lines without the use of Anderson's interruption procedure, new resonance functions were obtained in cases of strong (HF-HF) and weak (CO-CO) dipole-dipole, and dipole-quadrupole (HF-N_2) interactions.
2. Calculations of vibrotational line broadening coefficients and vibrational line shift coefficients of ozone molecule perturbed by nitrogen and oxygen were realized by the Robert–Bonamy formalism with exact trajectories and by the semi-empirical method; vibrationally dependent model isotropic potential was proposed.
3. Calculations of line shape parameters of vibrotational water vapour spectral lines induced by pressure of basic atmospheric gases N_2, O_2, H_2O were carried out. The semi-empirical method using results of variational calculations allowed determination of the line shape parameters up to the dissociation limit.
4. Effective values of the dipole polarizability of the water molecule in excited states were obtained for all vibrational bands experimentally studied in the literature.
5. The interference of water vapour lines for slanting and vertical paths leads to visible errors in calculations of the absorption coefficients for winter conditions of middle latitude atmosphere model and to disappearance of microwindow region with increasing zenithal angle.

List of publications

Articles

1*. A.D. Bykov, N.N. Lavrentieva, T.P. Mishina. "Generalized Euler series transformation applied to halfwidth and shift of molecular spectral lines calculation." // 15th Symposium on High-Resolution Molecular Spectroscopy (Proceedings Volume), **65800J**, 2006.

2*. A.D. Bykov, N.N. Lavrentieva, T.P. Mishina, L.N. Sinitsa, R.J. Barber, R.N. Tolchenov, J. Tennyson. "Water vapor line width and shift calculations with accurate vibration-rotation wave functions." // J. Quant. Spectrosc. Radiat. Transfer. 2008. **3034**. pp 1–11.

3*. A.D. Bykov, N.N. Lavrentieva, T.P. Mishina and L.N. Sinitsa "Influence of the Interference between Water Vapor Lines on the Atmospheric Transmission of Near-IR Radiation." // Optics and Spectroscopy. 2008, Vol. 104, No. 2, pp. 198-204.

4*. N.N. Lavrentieva, T.P. Mishina and L.N. Sinitsa, J. Tennyson. "Calculations of self-broadening and self-shifting of water vapor spectral lines with use of exact vibration-rotation wavefunctions." // Atm.Oceanic Optics, 21, N 12 (2008)

5*. A.D. Bykov, N.N. Lavrentieva, T.P. Mishina, L.N. Sinitsa, J. Tennyson. Line-broadening and shifting of water vapour: calculations with exact wave functions. // Optical spectroscopy and frequency standard. Atomic and molecular spectroscopy. / Ed. by L.N.

Sinitca and E.A. Vinogradov. – Tomsk: Publishing House of IAO SB RAS, 2009, Vol. 2, pp. 261-278

6*. J.V. Buldyreva, T.P. Mishina, N.N. Lavrentieva, A.S. Osipova Calculation of coefficients of collisional broadening of ozone spectral lines induced by pressure of atmospheric gases // Optics and Spectroscopy, 2010, Vol. 108, No 4, pp. 512-522

7*. B.A. Voronin, N.N. Lavrentieva, T.P. Mishina, T.Yu. Chesnokova, M.J. Barber, J. Tennyson. "Estimate of the J'J" dependence of water vapor line broadening parameters." // J. Quant. Spectrosc. Radiat. Transfer. 2010. **111**. pp 2308–2314.

8*. "The 2009 edition of the GEISA spectroscopic database" // Journal of Quantitative Spectroscopy and Radiative Transfer 2010 (in press)

Conference proceedings (books of abstracts)

9*. A.D. Bykov, N.N. Lavrentieva, T.P. Mishina "Effect of the interference of water vapor lines on the atmospheric transmittance." // XI Joint International Symposium "Atmospheric and Ocean Optics. Atmospheric Physics". – Tomsk: Institute of Atmospheric Optics SB RAS, 2004. – pp 200.

10*. A.D. Bykov, N.N. Lavrentieva, T.P. Mishina, V.N. Stroinova "Using of Generalized Euler Series Transformation for Calculation of Halfwidth and Shifts of Spectral Lines." // XIII International Symposium "Atmospheric and Ocean Optics. Atmospheric Physics". Abstracts. – Tomsk: Institute of Atmospheric Optics SB RAS, 2006. – pp 208.

11*. A.D. Bykov, N.N. Lavrentieva, T.P. Mishina "Using of Generalized Euler Series Transformation for Calculation of Halfwidth and Shifts of Molecular Spectral Lines." // XVth Symposium on High Resolution Molecular Spectroscopy HighRus-2006: Abstracts of Reports. – Tomsk: Institute of Atmospheric Optics SB RAS, 2006. – pp 190.

12*. A.D. Bykov, N.N. Lavrentieva, T.P. Mishina, L.N. Sinitsa "Water Vapor Line Pressure Broadening and Shift Calculations with Exact Vibration-Rotation Wave Functions." // XIV International Symposium "Atmospheric and Ocean Optics. Atmospheric Physics". Abstracts. – Tomsk: Institute of Atmospheric Optics SB RAS, 2007. – pp 250.

13*. N.N. Lavrentieva, T.P. Mishina, L.N. Sinitsa, J.Tennyson, and R.-J. Barber "Water vapor selfbroadening and selfshifting calculations with accurate vibration-rotation wave functions." // XV International Symposium "Atmospheric and Ocean Optics. Atmospheric Physics". Abstracts. – Tomsk: Institute of Atmospheric Optics SB RAS, 2008. – p. 47.

14*. T.P. Mishina, A.S. Osipova, J.V. Buldyreva, and N.N. Lavrentieva "Contour parameters of rotation-vibration ozone lines." // XV International Symposium "Atmospheric and Ocean Optics. Atmospheric Physics". Abstracts. – Tomsk: Institute of Atmospheric Optics SB RAS, 2008. – p. 53.

15*. T.P. Mishina, N.N. Lavrentieva, and B.A. Voronin. "Rotational Dependence of broadening coefficients of H2O spectral lines." // XV International Symposium "Atmospheric and Ocean Optics. Atmospheric Physics". Abstracts. – Tomsk: Institute of Atmospheric Optics SB RAS, 2008. – p. 55.

16*. B.A. Voronin, T.P. Mishina, N.N. Lavrentieva. "J-Dependence of broadening coefficients of H2O spectral lines." // Book of Abstracts of the 20th International Conference of High Resolution Molecular Spectroscopy, Prague, Czech Republic September 2-6, 2008. – p. 207.

17*. A.S. Osipova, T.P. Mishina, N.N. Lavrentieva, J.V. Buldyreva "Pressure Line Broadening of Asymmetric Top Molecules: O_3-N_2 (O_2)." // XVIth Symposium on High Resolution Molecular Spectroscopy HighRus-2009: Abstracts of Reports. – Tomsk: Institute of Atmospheric Optics SB RAS, 2009. – p. 103.

18*. B.A. Voronin, T.P. Mishina, N.N. Lavrentieva, T.Yu. Chesnokova, M.J. Barber, J. Tennyson. "JJ' Dependency of Broadening Coefficient for Water Vapor Transitions." // XVIth Symposium on High Resolution Molecular Spectroscopy HighRus-2009: Abstracts of Reports. – Tomsk: Institute of Atmospheric Optics SB RAS, 2009. – p. 91.

19*. T.P. Mishina, N.N. Lavrentieva, N.A. Lavrentiev Water vapor line broadening and shifting coefficients // XVI International Symposium "Atmospheric and Ocean Optics. Atmospheric Physics. - Tomsk: Institute of Atmospheric Optics SB RAS, 2009

20*. T.P. Mishina "Calculation of water vapor and ozone line broadening coefficients induced by nitrogen and oxygen pressure." // XI^{èmes} Journées des Écoles Doctorales Louis Paster – Université de Franche-Comté et Carnot – Université de Bourgogne – Besançon, **2010**.

21*. N.N. Lavrentieva, A.S. Osipova, T.P Mishina, J.V. Buldyreva Collisional ozone rovibrational line broadening induced by pressure of atmospheric gases // VII Russian Symposium «Control of environment and climate 2010» (Tomsk, 2010).

22*. A.S. Osipova, N.N. Lavrentieva, T.P. Mishina. Ozone rovibrational line shape parameters in 5 micrometer region // VIII International young scientists school «Environment physics» (Tomsk, 2010).

Oral presentations

1. T.P. Mishina, N.N. Lavrentieva. "Broadening of water vapour spectral lines: calculation with using of exact wave functions" // IV Russian conference "Material engineering, technologies and ecology in the 3^{d} millennium (Tomsk, 2009).

References

1. B.E. Grossman and E.V. Browell, J.Mol.Spectrosc.**136**, 264-294 (1989)
2. B.E. Grossman and E.V. Browell, J.Mol.Spectrosc.**138**, 562-595 (1989)
3. J.-P. Chevillard, J.-Y. Mandin, J.-M. Flaud, and C. Camy- Peyret, Can.J. Phys. **69**, 1286-1298 (1991)
4. K.M.T. Yamada, M. Harter, and T. Giesen. J. Mol. Spectrosc. **157**, 84-94 (1993)
5. D.C. Tobin, L.L. Strow, W.J. Lafferty, and W.B. Olson, Appl.Opt. **35,** 4724-4734 (1996)
6. R.A. Toth, J. Mol. Spectrosc., **201,** 218-243 (2000)
7. C.P. Rinsland, A. Goldman, M.A. Smith, and V.M. Devi, Appl.Opt. **30**, 1427-1438, (1991)
8. P.-F. Coheur, S. Fally, M. Carleer, C. Clerbaux, R Colin et al., J. Quant. Spectrosc. Radiat. Transfer, **749**, 493-510 (2002)
9. P.-F. Coheur, S. Fally, M. Carleer, C. Clerbaux, R Colin et al., J. Quant. Spectrosc. Radiat. Transfer, **82**, 119-131 (2003)
10. R.R. Gamache, J.-M. Hartmann, Can. J. Chem., **82**, 1013-1027 (2004)
11. P.W. Anderson, Phys. Rev. **76**, № 5, 657-661 (1949)
12. C.J. Tsao and B. Curnutte, J. Quant. Spectrosc. Radiat. Transfer, **2**, 41-91 (1962).
13. D. Robert and J. Bonamy, J. de Physique, **10**, 923–943 (1979).
14. C. Bloch, Nucl Phys. 1958; 7: 451-458
15. L.D. Landau, E.M. Lifshits, Cource of Theoretical Physics v.1, Pergamon, Oxford 1976
16. J. Buldyreva, J. Bonamy, D. Robert, JQSRT 62, 321 (1999) - linejnye molekuly
17. J. Buldyreva, S. Benec'h, M. Chrysos, Phys. Rev. A 63, 0123708 (2001) -sim. Tops
18. J. Buldyreva, L. Nguyen, Phys. Rev. A 77, 042720 (2008) - asim. tops
19. Q. Ma, R.H. Tipping, C. Boulet, J.Quant.Spectrosc.Radiat.Transfer. **103**, 588-596 (2007).
20. Q. Ma, R.H. Tipping, C. Boulet, J.Quant.Spectrosc.Radiat.Transfer. **243**, 105-112 (2007)
21. A. Bykov, N. Lavrentieva, L. Sinitsa, Mol. Phys. 102 (2004) 1653-1658
22. A. D. Bykov, N. N. Lavrentieva, L. N. Sinitsa, Atmos. Oceanic Opt. 5, 587-594 (1992)
23. R.P. Leavitt, J.Chem.Phys. 1980. V.73, №. 11. P. 5432-5448.
24. M.R. Cherkasov, Tomsk. 1975. 47 P. (in press №26 IAO SB AS USSR).
25. D. Korf, R.P. Leavitt, J.Chem.Phys. 1981.V.74.P.2180-2188.
26. A.D. Bykov, T.V. Kruglova, Atmos. Oceanic Opt. vol. 16, 2003, No.11, pp.924-927.
27. R.R. Gamache, E. Arie, C. Boursier, and J.M. Hartmann, Spectrochim. Acta A 54, 35-63 (1998).

28. A. Barbe, J.J. Plateaux, S. Bouazza, J.-M. Flaud, and C. Camy-Peyret, J.Quant.Spectrosc.Radiat.Transfer. **48**, 599-610 (1992).
29. J.E. Jones, Proc. R. Soc. A **106**, 463 (1924)
30. A. Barbe, S. Bouazza, J.J. Plateaux, Appl. Opt. 30 (1991) 2431-2436.
31. B.J, Drouin, J. Fischer, R.R. Gamache, J. Quant. Spectrosc. Radiat. Transfer, **83** (2004) 63-81
32. V.V. Zuev, Yu.N. Ponomarev, A.M. Solodov, B.A. Tikhomirov, and O.A. Romanovsky, Opt.Lett. **10,** 318-320 (1985)
33. H.Y. Mussa and J. Tennyson, J. Chem. Phys**., 109**, 10885-10892 (1998)
34. R.J. Barber, J. Tennyson, G.J. Harris and, R.N. Tolchenov, Mon. Not. R. Astr. Soc., **368**, 1087-1094 (2006)
35. J. Tennyson, M.A. Kostin, P. Barletta, G.J. Harris, J. Ramanalal, O.L. Polyansky and N.F. Zobov, Compt. Phys. Commun. **163**, 85 (2004)
36. S.V. Shirin, O.L. Polyansky, N.F. Zobov, P. Barletta and J. Tennyson, J. Chem. Phys., **118**, 2124 (2003)
37. D.W. Schwenke and H. Partridge, J. Chem. Phys. **113,** 6592 (2003)
38. S.L. Shostak, J.S. Muenter, J. Chem. Phys. **94**, 5883 (1991)
39. W.H. Flygare, R.C. Benson, Mol. Phys. **20**, 225 (1971)
40. W.F. Murphy, J.Chem.Phys. **67**, 5877 (1977)
41. P.-F. Coheur, S. Fally, M. Carleer, C. Clerbaux, R Colin et al., J. Quant. Spectrosc. Radiat. Transfer, **749**, 493-510 (2002)
42. P.-F. Coheur, S. Fally, M. Carleer, C. Clerbaux, R Colin et al., J. Quant. Spectrosc. Radiat. Transfer, **82**, 119-131 (2003)
43. S.A. Tashkun, V.I. Perevalov, J.-L. Teffo, A.D. Bykov, N.N. Lavrentieva, CDSD-1000, J. Quant. Spectrosc. Radiat. Transfer, **82**, 165-196 (2003)
44. R. Lynch, R.R. Gamache and S.P. Neshyba, J.Quant.Spectrosc.Radiat.Transfer. Vol 59, No 6. pp. 595-613, 1998.
45. A.D. Bykov, Yu.S. Makushkin, V.N. Stroinova, Opt. Spektrosk., **64**, 517-520 (1988)
46. M. R. Cherkasov, Opt. Spektrosk. **40** (1), 7 (1976)
47. F. Thibault, These de Docteur en Sciences, l'universite Paris XI Orsay, 1992
48. A.D. Bykov, N.N. Lavrent'eva, L.N. Sinitsa, and A.M. Solodov, Opt. Atmos. Okeana **14** (9), 846 (2001)
49. V.E. Zuev and V.S. Komarov, Statistical model of atmosphere temperature and gases components / Gidrometeoizdat, Leningrad, 1986 [in Russian].
50. I.I. Ippolitov, V.S. Komarov, and A.A. Mitsel', in *Spectroscopic Methods of Sounding of Atmosphere*, Ed. by I. V. Samokhvalov (Nauka, Novosibirsk, 1985) [in Russian]
51. A.D. Bykov, O. Naumenko, L. Sinitsa, et al., J. Mol. Spectrosc. **205** (1), 1 (2001)